A Curve-Fitting Approach to Estimate the Arterial Plasma Input Function for the Assessment of Glucose Metabolic Rate and Response to Treatment

Dennis Vriens, Lioe-Fee de Geus-Oei, Wim J.G. Oyen, and Eric P. Visser

Department of Nuclear Medicine, Radboud University Nijmegen Medical Center, Nijmegen, The Netherlands

For the quantification of dynamic ^{18}F-FDG PET studies, the arterial plasma time–activity concentration curve (APTAC) needs to be available. This can be obtained using serial sampling of arterial blood or an image-derived input function (IDIF). Arterial sampling is invasive and often not feasible in practice; IDIFs are biased because of partial-volume effects and cannot be used when no large arterial blood pool is in the field of view. We propose a mathematic function, consisting of an initial linear rising activity concentration followed by a triexponential decay, to describe the APTAC. This function was fitted to 80 oncologic patients and verified for 40 different oncologic patients by area-under-the-curve (AUC) comparison, Patlak glucose metabolic rate (MR_{glc}) estimation, and therapy response monitoring (ΔMR_{glc}). The proposed function was compared with the gold standard (serial arterial sampling) and the IDIF. **Methods:** To determine the free parameters of the function, plasma time–activity curves based on arterial samples in 80 patients were fitted after normalization for administered activity (AA) and initial distribution volume (iDV) of ^{18}F-FDG. The medians of these free parameters were used for the model. In 40 other patients (20 baseline and 20 follow-up dynamic ^{18}F-FDG PET scans), this model was validated. The population-based curve, individually calibrated by AA and iDV ($APTAC_{AA/iDV}$), by 1 late arterial sample ($APTAC_{1sample}$), and by the individual IDIF ($APTAC_{IDIF}$), was compared with the gold standard of serial arterial sampling ($APTAC_{sampled}$) using the AUC. Additionally, these 3 methods of APTAC determination were evaluated with Patlak MR_{glc} estimation and with ΔMR_{glc} for therapy effects using serial sampling as the gold standard. **Results:** Excellent individual fits to the function were derived with significantly different decay constants ($P < 0.001$). Correlations between AUC from $APTAC_{AA/iDV}$, $APTAC_{1sample}$, and $APTAC_{IDIF}$ with the gold standard ($APTAC_{sampled}$) were 0.880, 0.994, and 0.856, respectively. For MR_{glc}, these correlations were 0.963, 0.994, and 0.966, respectively. In response monitoring, these correlations were 0.947, 0.982, and 0.949, respectively. Additional scaling by 1 late arterial sample showed a significant improvement ($P < 0.001$). **Conclusion:** The fitted input function calibrated for AA and iDV performed similarly to IDIF. Performance improved significantly using 1 late arterial sample. The proposed model can be used when an IDIF is not available or when serial arterial sampling is not feasible.

Key Words: ^{18}F-FDG; positron emission tomography; chemotherapy; therapy monitoring; input function; theoretical models; pharmacokinetics; body fluid compartments; least-squares analysis; tissue distribution

Pharmacokinetic analysis of ^{18}F-FDG by dynamic PET requires both the arterial plasma time–activity concentration curve (APTAC, or $C_p(t)$ [input function]) and the tissue time–activity curve measured by PET (TTAC, or $C_T(t)$) to be available to create a Patlak plot (*1*) $\left(\frac{C_T(t)}{C_p(t)} \text{ vs. } \frac{\int_0^t C_p(\tau)d\tau}{C_p(t)} \right)$, from which the glucose metabolic rate (MR_{glc}) in the tissue of interest can be derived. Special interest in this type of quantitative analysis has risen for oncologic patients for prognostic stratification and response monitoring of disease.

The gold standard to obtain the APTAC is by measuring decay-corrected activity concentrations in plasma obtained by serial arterial sampling (*2*). This is an invasive and potentially harmful procedure for the patient and exposes the personnel to radiation. Complications attributed to radial artery cannulation include temporary occlusion (19.7%) and hematoma formation (14.4%), local infection (0.72%), sepsis (0.13%), permanent occlusion (0.09%), and pseudoaneurysm (0.09%) (*3*), some of which require medical intervention. Therefore, different methods have been developed to reduce these drawbacks. The major 4 alternatives to serial arterial sampling are (arterialized) venous blood sampling (*4,5*), image-derived input function (IDIF) estimation (*6–12*), population-based input function (*13–17*) modeling, and whole-blood input function extraction using sophisticated mathematic image segmentation methods (i.e., cluster analysis (*18*) and independent component analysis (*19–21*)).

A drawback of venous sampling is the time-dependent ratio of ^{18}F-FDG in venous to arterial blood (a ratio of 0.61–0.88 at 5–50 min after injection) (4,5). Therefore, shunting of arterial blood to the venous system (the heated-hand procedure) is used to improve these ratios to 0.92–1.05 (4). This arterialized venous sampling technique still requires cannulation of an extra vein and exposes personnel to radiation.

IDIFs require a large blood pool (aorta, left ventricle) within the field of view of the PET image. IDIFs show systematic error, because activity concentration is measured in whole blood, and activity concentration is known to be lower in whole blood than in plasma (ratio, ~0.925–0.95) (6–8). Moreover, partial-volume effects cause inaccuracy by spillover of activity from or to the surrounding tissues (e.g., myocardium) (6,9). Finally, additional noise is introduced because of the limited number of counts in the short early time frames. Because underestimation due to spill-out of the IDIF activity concentration leads to overestimation of MR_{glc} and overestimation due to spill-in of surrounding IDIF activity concentration (in later time frames) leads to underestimation of MR_{glc} (6,9), correction is necessary (10–12).

A population-based APTAC is based on the averaging of normalized sampled blood data of multiple patients. Several corrections were introduced, based on administered activity (AA), body weight, and blood transit time (13) or AA and body surface area (14,15). The latter provided a reliable estimation of MR_{glc} but yielded less accurate parameter values in pharmacokinetic analysis. Another method is the fitting of the sampled data to an equation, assuming the ^{18}F-FDG distribution in the vascular system as a compartment model on its own (16,17,22).

Here, we describe an APTAC model that is based on the fitting of a large series of arterially sampled oncologic patients to a mathematic equation (16,17,22). The model APTAC was calibrated to individual patients of a separate patient population by either an estimation of the distribution volume of ^{18}F-FDG (14,15) or 1 late arterial blood sample and compared with the gold standard of arterial sampling and the IDIF. The performance of both models was assessed by comparison of the APTACs themselves and by their influence on Patlak MR_{glc} and therapy response (ΔMR_{glc}) evaluation.

MATERIALS AND METHODS

Patient Population, Arterial Sampling Procedure

Data of 120 dynamic ^{18}F-FDG PET scans with serial arterial sampling data were reanalyzed. Scans were randomly distributed over 2 groups (Table 1): a parameter-identification group ($n = 80$) and a parameter-validation group ($n = 40$). For the latter group, both a pretreatment and a follow-up scan, after 2–3 courses of chemotherapy, were included. The details of ^{18}F-FDG PET and arterial plasma data acquisition are described elsewhere (9), with the only difference being that they were reconstructed using ordered-subsets expectation maximization with 4 iterations and 16 subsets with a gaussian filter of 5 mm in all directions. In short, normoglycemic patients who had fasted were injected with ^{18}F-FDG by an automated standardized infusion protocol. Directly thereafter, 17 arterial blood samples were taken at set time points from which plasma was obtained by centrifugation to provide a sampled arterial plasma time–activity concentration curve (APTAC$_{sampled}$). Simultaneously, dynamic PET, consisting of 16 time frames of variable length, was performed to provide both the tissue (TTAC) and the image-derived blood time–activity concentration curves (APTAC$_{IDIF}$).

TABLE 1. Comparison Between Parameter-Identification and Parameter-Validation Groups, with Statistical Significance of Group Difference

Parameter	Identification	Validation	P
PET scans (individual patients)	80 (49)	40 (20)	0.327*
Male sex (% of scans)	60	70	0.320*
Age (y)			0.225†
Median	60.7	60.1	
Range	44.8–78.9	44.7–71.9	
Mean administered activity ± SD (MBq)	207 ± 40.1	200 ± 35.8	0.314‡
Plasma glucose concentration (mmol·L^{-1})			0.125†
Median	5.3	5.3	
Range	4.2–10.0	4.2–8.3	
BMI (kg·m^{-2})			0.508†
Median	25.8	25.9	
Range	22.7–27.4	19.8–33.7	
Cancer localization (% of scans)			0.618*
Lung (non–small cell)	50	50	
Colorectal	45	40	
Breast	5	10	

*χ^2 test.
†Mann–Whitney U test.
‡Independent-samples t test.
BMI = body mass index.

Parameter-Identification Study ($n = 80$)

Normalization of the APTAC$_{sampled}$. The initial plasma concentration of ^{18}F-FDG ($C_p^*(0)$ [MBq·L^{-1}]) was used to normalize the APTAC$_{sampled}$. It was defined as the expected ^{18}F-FDG concentration directly after tracer injection, assuming instant homogenization, and is dependent on the AA (MBq) and the (apparent) initial distribution volume (iDV, [L]) (*14,15*). To avoid confusion, an "*" is added, because the sampled activity concentration at t = 0 is 0 MBq·L^{-1}.

In the period between 5 and 30 min after injection, the plasma and extravascular extracellular ^{18}F-FDG pool of the whole body were assumed to be in equilibrium (*23*). Before this period, the tracer is being distributed over the body, and in the period thereafter, the tracer is mainly being metabolized and excreted. Within this interval, we sampled 4 times (7.5, 12.5, 17.5, and 25 min after injection) (*9*) to obtain $C_p^*(0)$; semilogarithmic recordings of these 4 points were linearly extrapolated back to t = 0 (*y*-intercept) (*15,23*).

Estimation of iDV by Body Weight and Height. By definition, the iDV represents the (virtual) volume of the plasma and extravascular extracellular ^{18}F-FDG pool. The iDV can be estimated by (*14,15*):

$$iDV = \frac{AA}{C_p^*(0)} = c \cdot H^h \cdot W^w, \qquad \text{Eq. 1}$$

where H is patient height (m) and W is patient body weight (kg). Iteratively h, w, and c were derived for which the coefficient of variation of c ($CV_c = \frac{SD_c}{mean_c}$) is smallest in the parameter-identification data.

Fitting of Normalized APTAC$_{sampled}$. The normalized APTAC$_{sampled}$ can be approximated using the 3-compartment model for the blood pool as proposed by Feng et al. (*16*), simplified by Eberl et al. (*17*), as the following:

$$\frac{APTAC_{sampled}(t)}{C_p^*(0)} = \begin{cases} 0 & t < -\frac{b}{a} \\ a \cdot t + b & -\frac{b}{a} \leq t < \tau \\ \sum_{i=1}^{3} A_i \cdot e^{-\lambda_i \cdot (t - \tau)} & t \geq \tau \end{cases} \quad \text{Eq. 2}$$

where τ is the time to peak activity concentration. The normalized sampled plasma curves were fitted by linear curve fitting ($t < \tau$) and by nonlinear least squares ($t \geq \tau$) to obtain the 8 free parameters in every patient of the parameter-identification study. Because chemotherapy might influence ^{18}F-FDG distribution and clearance, the parameter values were compared between scans made in patients who did and did not receive chemotherapy.

Parameter-Validation Study ($n = 40$)

IDIF and Tumor Time–Activity Curves. The APTAC$_{IDIF}$ was determined in manually placed volumes of interest (VOIs) over the ascending aorta (thoracic images) or descending aorta (abdominal images) known to correlate best with the gold standard (*9*) on summed images of the period 30–90 s after injection. The TTAC was obtained semiautomatically by placing volumes of interest in the summed images of the period 20–50 min after injection over the largest lesion, fully present in the field of view, using a threshold of 50% of its maximum voxel value. All images were analyzed using the Inveon Research Workplace (version 2.2; Siemens).

Comparison of Calibrated Plasma Time–Activity Curves and Glucose Metabolic Rates. Median values of APTAC parameters derived from the parameter-identification study were used for the population-based APTAC, which was calibrated to each individual patient, using 2 methods: by either multiplication by AA (MBq) divided by iDV (L) (estimated using Eq. 1, further mentioned as APTAC$_{AA/iDV}$) or multiplication by the plasma activity concentration of 1 late arterial sample (APTAC$_{1sample}$).

The performance of the 3 curves (APTAC$_{AA/iDV}$, APTAC$_{1sample}$, and APTAC$_{IDIF}$) was compared with that of the gold standard (APTAC$_{sampled}$) by their area under the curve (AUC), determined by trapezoid integration.

MR$_{glc}$ was determined using all 4 plasma input curves by Patlak graphical analysis (*1*). In the Patlak approximation, the lumped constant, accounting for the difference in glucose and ^{18}F-FDG affinity, was set to 1 and the tumor blood fraction was set to 0. Therefore, the slope of the Patlak plot was K_i and the intercept was $\frac{K_1 \cdot k_2}{(k_2 + k_3)^2}$. MR$_{glc}$ can then be determined by multiplying the linear regression (5–50 min after injection) by the plasma glucose concentration.

Statistical Analysis

All variables were assessed for normality (Shapiro–Wilk, skewness, and kurtosis) and are either displayed as mean ($\pm$SD) or median (interquartile range). Comparison between 2 independent groups was performed by the *t* test, the Mann–Whitney *U* test, or the χ^2 test. λ_1–λ_3 were compared using Friedman ANOVA. Correlations between the AUC, MR$_{glc}$, and ΔMR$_{glc}$ of the different curves compared with the gold standard were assessed by Pearson *r* or Spearman ρ and linear regression and are displayed as Bland–Altman plots. Confidence intervals for correlation coefficients were compared after Fisher *z* transformation (*24*). Analysis was performed by SPSS 16.0.2 (SPSS Inc.). Two-sided significance was set at the 0.050 level.

RESULTS

Parameter-Identification Study

A median iDV of 12.7 L (corresponding to 0.1683 L/kg body weight) was calculated. Iterative determination of the function to estimate the iDV led to h = 1.257, w = 0.582, and c = 0.533 L·m$^{-1.257}$·kg$^{-0.582}$ (minimum CV$_c$, 0.171; adjusted R^2, 0.3181).

Fitting of the 80 APTAC$_{sampled}$ by Equation 2 led to a minimum adjusted R^2 of 0.8533; 80% of fits had an adjusted R^2 greater than 0.9500. Resulting parameters for the normalized APTAC$_{sampled}$ are provided in Table 2. No significant difference in ^{18}F-FDG clearance could be detected ($P > 0.326$) between patients who did and did not receive chemotherapy. The 3 decay constants (λ_1–λ_3) were significantly different ($P < 0.001$; Fig. 1).

Parameter-Validation Study

The correlation between the AUC of the APTAC$_{AA/iDV}$ and the APTAC$_{sampled}$ was 0.880. This correlation improved to 0.994 ($P < 0.001$) using 1 arterial sample for calibration. The mean AUC of APTAC$_{AA/iDV}$ was similar to (462 $\pm$ 119 MBq·L^{-1}·min), and that of APTAC$_{1sample}$ slightly lower than (468 $\pm$ 107 MBq·L^{-1}·min), the gold standard (APTAC$_{sampled}$, 475 $\pm$ 108 MBq·L^{-1}·min,

TABLE 2. Results of Fitting of Normalized Plasma Data of Parameter-Identification Group and Subgroup Analysis Between Pretherapy Scans and Posttherapy Scans

Parameter	All scans ($n = 80$)		Pretherapy scans ($n = 40$)		Follow-up scans ($n = 40$)		
	Median	IQR	Median	IQR	Median	IQR	P^*
τ (min)	1.25	1.25–1.50	1.25	1.25–1.25	1.25	1.25–1.50	0.077
a (min^{-1})	4.911	4.188–5.709	4.914	4.154–5.660	4.911	4.203–5.771	0.672
b	−2.077	−2.817 to −1.321	−1.195	−2.805 to −1.096	−2.225	−2.961 to −1.503	0.168
A_1	2.785	2.302–3.212	2.718	2.241–3.152	2.937	2.321–3.300	0.326
λ_1 (min^{-1})	6.133	4.646–8.114	6.034	4.121–8.064	6.133	4.833–8.322	0.622
A_2	0.7085	0.6492–0.8011	0.6966	0.6340–0.8434	0.7229	0.6694–0.8130	0.589
λ_2 (min^{-1})	0.2541	0.2075–0.3071	0.2400	0.1881–0.3423	0.2592	0.2285–0.2847	0.805
A_3	0.7721	0.7177–0.8070	0.7699	0.6861–0.8286	0.7741	0.7385–0.7970	0.920
λ_3 (min^{-1})	0.01443	0.01248–0.01595	0.01446	0.01206–0.01656	0.01434	0.01260–0.01590	0.562

*Mann–Whitney U test.
IQR = interquartile range.

$P = 0.156$ and $P < 0.001$, respectively). The APTAC$_{IDIF}$ showed much lower AUCs than APTAC$_{sampled}$ (392 ± 99 MBq·L^{-1}·min, $P < 0.001$), with a correlation coefficient between these parameters of 0.856.

Comparison between MR$_{glc}$ is shown in Figure 2 (left panels). Adding 1 arterial sample (25 min after injection) improved the correlation between MR$_{glc}$, determined by APTAC$_{AA/iDV}$ and APTAC$_{sampled}$, from $\rho = 0.963$ to $\rho = 0.994$ ($P < 0.001$). MR$_{glc}$ determined by IDIF was significantly higher than the gold standard; the correlation was similar to that of APTAC$_{AA/iDV}$ ($\rho = 0.966$).
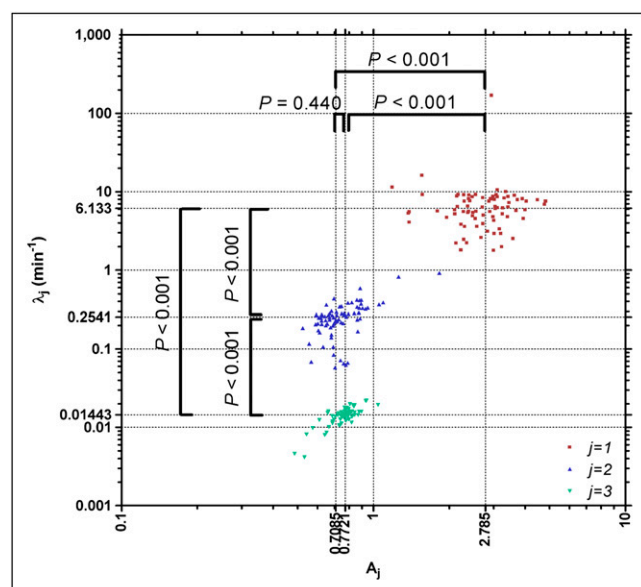
Comparison between therapy effects (ΔMR$_{glc}$) is shown in Figure 2 (right panels). Adding 1 arterial sample (25 min after injection) improved the correlation between ΔMR$_{glc}$ determined by APTAC$_{AA/iDV}$ and APTAC$_{sampled}$ from $\rho =$

0.947 to $\rho = 0.982$ ($P = 0.012$). ΔMR$_{glc}$ determined by APTAC$_{IDIF}$ had a correlation to the gold standard similar to that determined by APTAC$_{AA/iDV}$ ($\rho = 0.949$).

Any arterial sample taken at 7.5 min after injection showed similar high correlations when comparing MR$_{glc}$ ($\rho \geq 0.9916$) or ΔMR$_{glc}$ ($\rho \geq 0.9759$) measured by APTAC$_{sampled}$ and APTAC$_{1sample}$.
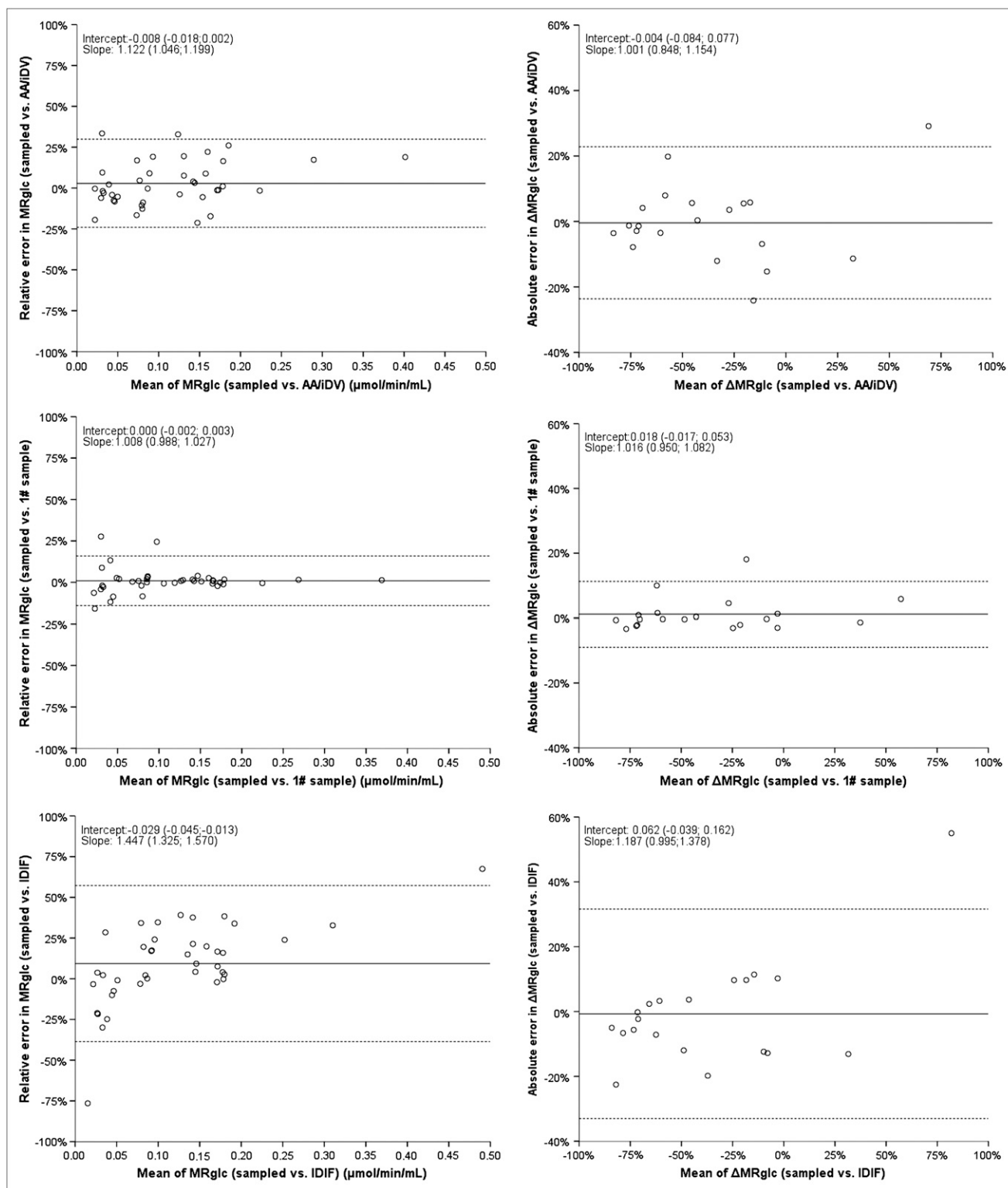
DISCUSSION

This study describes the performance of a population-based APTAC based on fitting patient data to a mathematic equation on Patlak determination of MR$_{glc}$ and on chemotherapy response evaluation. Its accuracy is comparable to that of an IDIF, explaining 93% of variance in MR$_{glc}$ (90% in response evaluation by ΔMR$_{glc}$), but the addition of 1 late arterial sample improves this to 99% (96% in response evaluation by ΔMR$_{glc}$). Where the IDIF is fully individual, the proposed method is a population average, calibrated to individual patient parameters without the need for serial arterial sampling. The method can be used when scanning body regions where blood pools are unavailable, such as the extremities. The model can be further improved by including 1 arterial sample. It can be expected that a late arterialized venous sample might adequately replace the arterial sample, because more than approximately 30 min after ^{18}F-FDG injection, activity concentrations of arterial and arterialized venous blood are highly similar (4,5). This sample might also be used to obtain an accurate measurement of the plasma glucose level, as long as radiation safety regulations do not prohibit this analysis in the clinical chemistry laboratory. As shown, MR$_{glc}$ was significantly overestimated using an IDIF, compared with the gold standard. Both the partial-volume effect and the fact that whole-blood activity concentrations are lower than in plasma cause underestimation of the (integral of the) APTAC. From the Patlak equation it can be derived that an underestimation of the APTAC and its integral cause overestimation of the MR$_{glc}$. The quality of the IDIF can be

FIGURE 1. Scatter plot of $\log_{10}(A_j)$ vs. $\log_{10}(\lambda_j)$, showing clustering of 3 decay constants.

FIGURE 2. Bland–Altman plots of comparison between any of 3 evaluated APTACs and gold standard. In Bland–Altman plots, mean difference is displayed by solid line and 95% confidence interval by dotted lines. Unstandardized regression coefficients are displayed with corresponding 95% confidence interval. 1# sample was calibrated by 1 arterial sample at 25 min after injection; AA/iDV was calibrated by AA and iDV.

improved by correction for the partial-volume and spillover effects (25). Moreover, the activity in whole blood can be corrected to the activity concentration in plasma using hematocrit (19) or modeled erythrocyte uptake (26). In addition, the noise in the short early time frames contributes to the inaccuracy of the activity concentration. Recently, 8 methods for the estimation of the carotid IDIF in human brain studies were compared with the reference input function (arterially sampled) with respect to cerebral MR_{glc} and individual rate constants in a study consisting of phantoms and healthy volunteers. The authors concluded that blood-sample–free methods provided less reliable results than those obtained using the methods that require blood samples, even when limited to a single sample (27). Therefore, calibration of our IDIFs by 1 late venous sample would probably have improved the accuracy of these IDIFs. The advantage of a more patient-specific rather than a generic input function is especially important for pharmacokinetic analysis, because the exact shape of the APTAC in the artery feeding the tumor is vital and is usually different from a remote artery (because of delay and dispersion by the intraindividual variation in the impulse-response characteristics of the vascular system).

One method of calibration of the population-based curve was by the approach of Sadato et al. (23) (AA/iDV). They reported a mean iDV scaled to body weight (iDV_{BW}) of 0.1627 $L \cdot kg^{-1}$, similar to this study (median iDV_{BW} of 0.1683 $L \cdot kg^{-1}$). Around 50%−60% of the body weight of an average adult is water, of which 25%−45% (0.18 $L \cdot kg^{-1}$) is extracellular fluid (the volume of water in which ^{18}F-FDG dissolves), stressing both the concordance and plausibility of this result (28). We used the function of Shiozaki et al. (15) to fit the iDV. They reported an iDV[mL] that equaled $39.0 \cdot H[cm]^{0.80} \cdot W[kg]^{0.35}$. This result appears different from the present study (iDV[L] = $0.533 \cdot H[m]^{1.257} \cdot W[kg]^{0.582}$), but they were only slightly off our optimum (CV_c = 0.18 vs. CV_c = 0.17). A dissimilar distribution of body habitus in their (Asian) population might be the cause for this difference.

As shown in Figure 2, the difference between MR_{glc} calculated by $APTAC_{1sample}$ and $APTAC_{sampled}$ was small; therefore, the net influx constant determined by Patlak analysis was accurate. For determining the individual rate constants, however, the inaccuracy will probably be much higher. For Patlak analysis, only the integral of the APTAC and the late (>5 min) activity concentrations of the arterial plasma are relevant, but for the accurate estimation of the individual rate constants of glucose pharmacokinetics, the exact shape of the APTAC is vital, because of both the function (including a convolution operation) and the method for parameter estimation (nonlinear least squares). The delay and dispersion between the APTAC in the artery feeding the tissue of interest and a remote artery are of major importance for the accurate determination of the fast rate constants (K_1 and k_2) and blood fraction (V_b). Moreover, the use of a generic input function for pharmacokinetic analysis should be considered because of the large intraindividual variation of the slow clearance rate constants of ^{18}F-FDG (λ_3 [and to a lesser extent in λ_2] in Fig. 1 and Table 2). The assumption of a single clearance profile for all patients might therefore lead to the inaccurate estimation of the slower rate constants (k_3 and, if it exists, k_4) of individual patients.
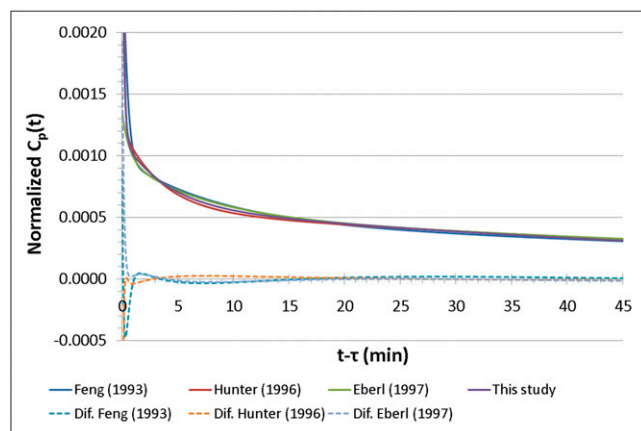
The proposed model, therefore, should be evaluated further for estimating microparameters before implementation. This further evaluation, however, was out of the scope of this study.

None of the previously published articles on population-based input curves used an IDIF for comparison, and most studies consisted of a small series of nononcologic patients, but reproducibility was high (Table 3). The studies that used triexponential clearance of ^{18}F-FDG as a function for the APTAC (16,17,22) found a decay similar to that found in this study (Fig. 3). The results shown in Figure 1 suggest a high (linear) correlation between A_3 and λ_3. This correlation suggests that the model might be simplified by omitting 1 parameter; we did not verify the possibility of simplifying the model in this study.

TABLE 3. Literature Review of Publications on Population-Based APTACs and IDIFs

Reference	n	Method	Calibration	AUC	MR_{glc}
Takikawa et al. (13)	10/24	Arithmetic mean	2 arterial	0.998	0.992
			1 AVS	0.998	0.989
Tsuchida et al. (14)	44/10	Arithmetic mean	—	+3.5% ± 2.2%	+2.9% ± 1.9%
Shiozaki et al. (15)	101/192	Arithmetic mean	AA/iDV	+7.2% ± 5.7%	+8.9% ± 7.3%
Bentourkia et al. (29)	20/same 20	Fit to equation	—	—	0.998
Eberl et al. (17)	26/26	Fit to equation	2 AVS	—	0.995
de Geus-Oei et al. (9)	136	IDIF	—	—	0.98
This study	80/40	Fit to equation	AA/iDV	0.880	0.963
			1 arterial	0.994	0.994
		IDIF	—	0.856	0.966

———

n = no. of patients (to derive curve/to validate curve); AUC = correlation or mean % difference between AUC of population-based curve and serial arterial sampling; MR_{glc} = correlation or mean % difference between glucose metabolic rate of population-based curve and serial arterial sampling; AVS = arterialized venous samples; AA/iDV = administered activity/initial distribution volume of ^{18}F-FDG.

FIGURE 3. Comparison of triexponential ^{18}F-FDG clearance in our study and 3 previous publications (*16,17,22*). Functions were normalized to total AUC. Dif. = absolute differences of our clearance curve compared with 3 found in literature.

CONCLUSION

The current model of the APTAC of ^{18}F-FDG, calibrated by 1 late arterial sample, shows high accuracy for Patlak MR$_{glc}$ calculation and treatment response monitoring. The model allows dynamic scanning of areas without large vessels in the field of view, such as the extremities; is less invasive; and causes less radiation exposure to personnel than does arterial sampling. Even without a calibrating sample available, this model has the same accuracy as an IDIF, without its inherent disadvantages.

REFERENCES

1. Patlak CS, Blasberg RG, Fenstermacher JD. Graphical evaluation of blood-to-brain transfer constants from multiple-time uptake data. *J Cereb Blood Flow Metab.* 1983;3:1–7.
2. Greuter HN, Boellaard R, van Lingen A, Franssen EJ, Lammertsma AA. Measurement of ^{18}F-FDG concentrations in blood samples: comparison of direct calibration and standard solution methods. *J Nucl Med Technol.* 2003;31:206–209.
3. Scheer B, Perel A, Pfeiffer UJ. Clinical review: complications and risk factors of peripheral arterial catheters used for haemodynamic monitoring in anaesthesia and intensive care medicine. *Crit Care.* 2002;6:199–204.
4. van der Weerdt AP, Klein LJ, Visser CA, Visser FC, Lammertsma AA. Use of arterialised venous instead of arterial blood for measurement of myocardial glucose metabolism during euglycaemic-hyperinsulinaemic clamping. *Eur J Nucl Med Mol Imaging.* 2002;29:663–669.
5. Wakita K, Imahori Y, Ido T, et al. Simplification for measuring input function of FDG PET: investigation of 1-point blood sampling method. *J Nucl Med.* 2000;41:1484–1490.
6. van der Weerdt AP, Klein LJ, Boellaard R, Visser CA, Visser FC, Lammertsma AA. Image-derived input functions for determination of MRGlu in cardiac ^{18}F-FDG PET scans. *J Nucl Med.* 2001;42:1622–1629.
7. Dhawan V, Takikawa S, Robeson W, et al. Quantitative brain FDG/PET studies using dynamic aortic imaging. *Phys Med Biol.* 1994;39:1475–1487.
8. Ohtake T, Kosaka N, Watanabe T, et al. Noninvasive method to obtain input function for measuring tissue glucose utilization of thoracic and abdominal organs. *J Nucl Med.* 1991;32:1432–1438.
9. de Geus-Oei LF, Visser EP, Krabbe PF, et al. Comparison of image-derived and arterial input functions for estimating the rate of glucose metabolism in therapy-monitoring ^{18}F-FDG PET studies. *J Nucl Med.* 2006;47:945–949.
10. Lin KP, Huang SC, Choi Y, Brunken RC, Schelbert HR, Phelps ME. Correction of spillover radioactivities for estimation of the blood time-activity curve from the imaged LV chamber in cardiac dynamic FDG PET studies. *Phys Med Biol.* 1995;40:629–642.
11. Gambhir SS, Schwaiger M, Huang SC, et al. Simple noninvasive quantification method for measuring myocardial glucose utilization in humans employing positron emission tomography and fluorine-18 deoxyglucose. *J Nucl Med.* 1989;30:359–366.
12. Chen K, Bandy D, Reiman E, et al. Noninvasive quantification of the cerebral metabolic rate for glucose using positron emission tomography, ^{18}F-fluoro-2-deoxyglucose, the Patlak method, and an image-derived input function. *J Cereb Blood Flow Metab.* 1998;18:716–723.
13. Takikawa S, Dhawan V, Spetsieris P, et al. Noninvasive quantitative fluorodeoxyglucose PET studies with an estimated input function derived from a population-based arterial blood curve. *Radiology.* 1993;188:131–136.
14. Tsuchida T, Sadato N, Yonekura Y, et al. Noninvasive measurement of cerebral metabolic rate of glucose using standardized input function. *J Nucl Med.* 1999;40:1441–1445.
15. Shiozaki T, Sadato N, Senda M, et al. Noninvasive estimation of FDG input function for quantification of cerebral metabolic rate of glucose: optimization and multicenter evaluation. *J Nucl Med.* 2000;41:1612–1618.
16. Feng D, Huang SC, Wang X. Models for computer simulation studies of input functions for tracer kinetic modeling with positron emission tomography. *Int J Biomed Comput.* 1993;32:95–110.
17. Eberl S, Anayat AR, Fulton RR, Hooper PK, Fulham MJ. Evaluation of two population-based input functions for quantitative neurological FDG PET studies. *Eur J Nucl Med.* 1997;24:299–304.
18. Liptrot M, Adams KH, Martiny L, et al. Cluster analysis in kinetic modelling of the brain: a noninvasive alternative to arterial sampling. *Neuroimage.* 2004;21:483–493.
19. Su KH, Wu LC, Liu RS, Wang SJ, Chen JC. Quantification method in [^{18}F]fluorodeoxyglucose brain positron emission tomography using independent component analysis. *Nucl Med Commun.* 2005;26:995–1004.
20. Naganawa M, Kimura Y, Ishii K, Oda K, Ishiwata K, Matani A. Extraction of a plasma time-activity curve from dynamic brain PET images based on independent component analysis. *IEEE Trans Biomed Eng.* 2005;52:201–210.
21. Chen K, Chen X, Renaut R, et al. Characterization of the image-derived carotid artery input function using independent component analysis for the quantitation of [^{18}F] fluorodeoxyglucose positron emission tomography images. *Phys Med Biol.* 2007;52:7055–7071.
22. Hunter GJ, Hamberg LM, Alpert NM, Choi NC, Fischman AJ. Simplified measurement of deoxyglucose utilization rate. *J Nucl Med.* 1996;37:950–955.
23. Sadato N, Tsuchida T, Nakaumra S, et al. Non-invasive estimation of the net influx constant using the standardized uptake value for quantification of FDG uptake of tumours. *Eur J Nucl Med.* 1998;25:559–564.
24. Fisher RA. On the 'probable error' of a coefficient of correlation deduced from a small sample. *Metron.* 1921;1:3–32.
25. Fang YH, Muzic RF Jr. Spillover and partial-volume correction for image-derived input functions for small-animal ^{18}F-FDG PET studies. *J Nucl Med.* 2008;49:606–614.
26. Lee JS, Su KH, Lin JC, et al. A novel blood-cell-two-compartment model for transferring a whole blood time activity curve to plasma in rodents. *Comput Methods Programs Biomed.* 2008;92:299–304.
27. Zanotti-Fregonara P, Fadaili EM, Maroy R, et al. Comparison of eight methods for the estimation of the image-derived input function in dynamic [^{18}F]-FDG PET human brain studies. *J Cereb Blood Flow Metab.* July 8, 2009 [Epub ahead of print].
28. Singer GG, Brenner BM. Chapter 46. Fluid and electrolyte disturbances. In: Fauci AS, Braunwald E, Kasper DL, et al., eds. *Harrison's Principles of Internal Medicine.* 17th ed. Columbus, OH: McGraw-Hill Companies; 2008:274–285.
29. Bentourkia M, Bol A, Ivanoiu A, et al. A standardized blood sampling scheme in quantitative FDG-PET studies. *IEEE Trans Med Imaging.* 1999;18:379–384.

The Journal of NUCLEAR MEDICINE

A Curve-Fitting Approach to Estimate the Arterial Plasma Input Function for the Assessment of Glucose Metabolic Rate and Response to Treatment

Dennis Vriens, Lioe-Fee de Geus-Oei, Wim J.G. Oyen and Eric P. Visser

This article and updated information are available at:
http://jnm.snmjournals.org/content/50/12/1933

Information about reproducing figures, tables, or other portions of this article can be found online at:
http://jnm.snmjournals.org/site/misc/permission.xhtml

Information about subscriptions to JNM can be found at:
http://jnm.snmjournals.org/site/subscriptions/online.xhtml

SOCIETY OF
NUCLEAR MEDICINE
AND MOLECULAR IMAGING